Spatial interactions modulate tumor growth and immune infiltration

Jeffrey West

jeffrey.west@moffitt.org

Moffitt Cancer Center   https://orcid.org/0000-0001-9579-4664

Sadegh Marzban

H. Lee Moffitt Cancer Center & Research Institute

Sonal Srivastava

H. Lee Moffitt Cancer Center & Research Institute

Sharon Kartika

Indian Institute of Science Education and Research Kolkata

Rafael Bravo

Moffitt Cancer Center

Rachel Safriel

High School Internship Program, H. Lee Moffitt Cancer Center & Research Institute

Aidan Zarski

High School Internship Program, H. Lee Moffitt Cancer Center & Research Institute

Alexander Anderson

H. Lee Moffitt Cancer Center & Research Institute   https://orcid.org/0000-0002-2536-4383

Christine Chung

H. Lee Moffitt Cancer Center & Research Institute

Antonio Amelio

H. Lee Moffitt Cancer Center & Research Institute

Additional Declarations: There is **NO** Competing Interest.

Spatial interactions modulate tumor growth and immune infiltration

Sadegh Marzban[1], Sonal Srivastava[2], Sharon Kartika[3], Rafael Bravo[1], Rachel Safriel[4], Aidan Zarski[4], Alexander Anderson[1], Christine H. Chung[5], Antonio L. Amelio[2,5], and Jeffrey West[1,*]

[1]Integrated Mathematical Oncology Dept., H. Lee Moffitt Cancer Center & Research Institute, Tampa, FL
[2]Dept. of Tumor Microenvironment and Metastasis, H. Lee Moffitt Cancer Center & Research Institute, Tampa, FL
[3]Dept. of Biological Sciences, Indian Institute of Science Education and Research Kolkata
[4]High School Internship Program, H. Lee Moffitt Cancer Center & Research Institute, Tampa, FL
[5]Dept. of Head and Neck-Endocrine Oncology, H. Lee Moffitt Cancer Center & Research Institute, Tampa, FL

[*]**jeffrey.west@moffitt.org**

ABSTRACT

Lenia, a cellular automata framework used in artificial life, provides a natural setting to implement mathematical models of cancer incorporating features such as morphogenesis, homeostasis, motility, reproduction, growth, stimuli response, evolvability, and adaptation. Historically, agent-based models of cancer progression have been constructed with rules that govern birth, death and migration, with attempts to map local rules to emergent global growth dynamics. In contrast, Lenia provides a flexible framework for considering a spectrum of local (cell-scale) to global (tumor-scale) dynamics by defining an interaction kernel governing density-dependent growth dynamics. Lenia can recapitulate a range of cancer model classifications including local or global, deterministic or stochastic, non-spatial or spatial, single or multi-population, and off or on-lattice. Lenia is subsequently used to develop data-informed models of 1) single-population growth dynamics, 2) multi-population cell-cell competition models, and 3) cell migration or chemotaxis. Mathematical modeling provides important mechanistic insights. First, short-range interaction kernels provide a mechanism for tumor cell survival under conditions with strong Allee effects. Next, we find that asymmetric interaction tumor-immune kernels lead to poor immune response. Finally, modeling recapitulates immune-ECM interactions where patterns of collagen formation provide immune protection, indicated by an emergent inverse relationship between disease stage and immune coverage.

1 Introduction

L ENIA (from the Latin *lenis* meaning "smooth") is a cellular automata framework that allows for continuous space and time. Cellular automata are often used to study the "rules" that can recapitulate the collective behavior of interacting biological "agents" (e.g. individual cells or organisms). The development of Lenia was spurred by the search for rule-sets that lead to features that are important in artificial life: self-organization (morphogenesis) self-regulation (homeostasis), self-direction (motility), self-replication (reproduction), growth (development), response to stimuli or environmental factors, evolvability, adaptation[1, 2], and other emergent complexity[3].

Many of these same features (e.g. cellular replication, growth, motility, evolvability, and adaptation) are important in the development of complex, multi-factorial diseases such as cancer. Thus, the purpose of this manuscript is to extend the Lenia framework as a tumor model, including immune predation and escape. We show how this is a natural extension, as Lenia has the capability to recapitulate 1) classical

analytical models of cancer (ordinary differential equations), 2) common stochastic agent-based models of cancer, 3) standard models of multiple cell types competing on a Darwinian fitness landscapes (evolutionary game theory), and 4) generalized cell migration (e.g. chemotaxis models) common in cancer mathematical modeling literature.

1.1 The overlap in modeling artificial life and cancer evolution

In its original formulation, Lenia defines an on-lattice domain where each grid location can take a continuous density value. Methods of interactive evolutionary computation were used to find rule-sets that lead to defined, artificial "creatures" (see figure 1A for examples) which are capable of stable linear or angular motion or other life-like characteristics (figure 1B)[1,2]. These continuous creatures are reminiscent of the binary gliders, oscillators, and still-life creatures in Conway's Game of Life[4].

Grid locations change according to an update rule describing the growth dynamics (figure 1C) paired with an interaction kernel function (figure 1D). For example, tumor cell density in a two-dimensional domain (figure 1E) is convolved with an interaction kernel (figure 1F) to calculate the "density potential" (figure 1G). Density potential is the surrounding density of grid locations weighted by kernel interaction function of radial distance from the focal cell. This defines a spatially-explicit growth field (figure 1H)[1], whereby the update rule is enacted iteratively at each time step, t (figure 1I). Thus, a natural interpretation of Lenia as a cancer model is a spatial density map of cancer cells. Cancer cells grow according to a local density-dependent growth rate (e.g. logistic growth) which is a function of local cell density. Lenia can compare the effect of local (short-range kernels) versus global (long-range kernels) on growth dynamics.

There exists broad overlap in both methods and desired emergent behavior between models of artificial life and models of cancer growth (figure 1H). To adequately mimic biological realism in cancer, mathematical frameworks have implemented methods classified as 1) non-spatial or spatial, 2) deterministic or stochastic, and 3) single or multiple populations (cell types). Lenia allows for flexible model design to incorporate the full range of these classifications. Extensions to Lenia include Glaberish (a variant that leads to pattern formations that are stable in space or time[5]), Flow-Lenia (imposes mass conservation over time)[6], Asymptotic-Lenia (asymptotic, smooth updating)[7], Particle-Lenia (off-lattice)[8], or a generalized reaction-diffusion implementation[9].
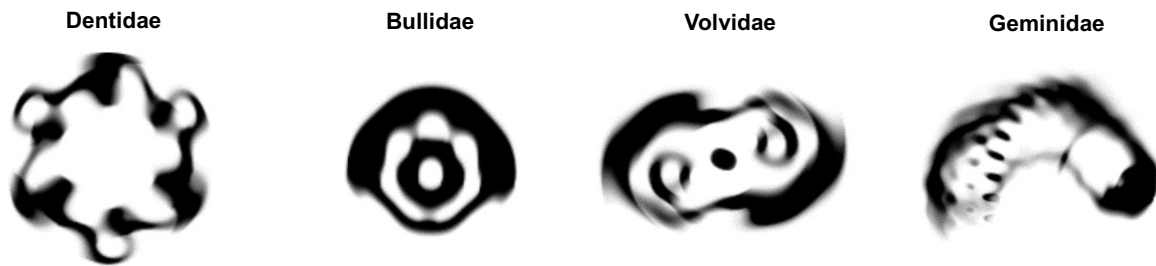
1.2 Modeling spatial effects in tumor-immune dynamics

Spatio-temporal models of cancer growth dynamics

Tumor growth can be expressed as a mathematical law using an ordinary differential equation (ODE)[10] and used as a predictive tool in assessing the course of tumor progression[11,12]. ODE frameworks use the well-mixed assumption, where each cell is equally likely to interact with each other cell in the tumor. Thus, there is a broad interest in understanding the effect of local, cell-scale contact inhibition on the emergent tumor-scale global growth dynamics[13–15]. The choice of spatial structure within a model (e.g. non-spatial, deme models, mesoscale, or boundary-driven growth) affects the evolutionary dynamics within heterogeneous tumors[16–19], tumor growth dynamics[20,21] and the emergent pattern formation[22–24].

Lenia is classified as a system of integro-differential equations (IDE)[25]. IDEs have been used to study cancer progression[26] and treatment[27] or to find approximations of stochastic ABMs in cancer[28], but these formulations often focus on how interaction kernels alter the time scale of dynamics or the system stability. Lenia provides a unifying framework for direct comparison of well-mixed assumptions commonly used in ODE models (corresponding to Lenia's long-range kernel) and local-scale competition commonly used in stochastic agent-based modeling (corresponding to Lenia's short-range kernels).
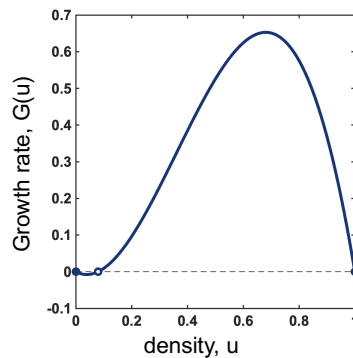
Figure 1. Lenia as a cancer model: (A) Lenia artificial life virtual creatures, reproduced from ref. 1. (B) List of characteristics possible to produce in Lenia by varying the growth dynamics function (C) or the interaction kernel function (D). (E) An example snapshot of a simulation shows the density of cells at each lattice location where the interaction kernel (F) specifies the nature of interaction of cells depending on their distance from each other. (G) The density potential, interpreted as a weighted average of interactions at each lattice location, is calculated as the convolution of $\mathbf{A}(\mathbf{x})$ and $\mathbf{K}(\mathbf{x})$. (H) the growth field calculated by applying a growth map to the density potential. (I) adding a fraction of the growth field at each time step to the cell density, forms the Lenia update rule, as seen in eqn. 1.

Spatio-temporal models of tumor-immune interactions

Tumors do not grow in isolation but must develop immune escape mechanisms to avoid extinction. Tumor-immune interactions have been described using logistic tumor growth with immune recruitment and exhaustion[29] or as a predator-prey relationship[30]. Immune predation has likewise been modelled using integro-differential equations[31–34], mesoscopic models[35], or stochastic agent-based methods[36].

Importantly, classical predator-prey models may be insufficient to describe tumor-immune dynamics without also considering mechanisms for avoiding oscillatory behavior common to these models[37]. Thus, in the models developed herein we include Allee effects, whereby tumors require a cooperative benefit of close aggregation when at lower densities[38,39]. Allee effects lead to a decreased growth benefit when tumor density is low, and thus are proposed to enable immune predation to fully eliminate tumors in the absence of immune escape[37].

Spatio-temporal models of cell migration and the extracellular matrix

Cell migration is influenced by the spatial configuration of collagen[40,41]. The density, orientation, and thickness of collagen fibers within the extracellular matrix (ECM) can influence migration through contact guidance thereby facilitating both migration and invasion[42]. Much of the mathematical modeling in this area focuses on recapitulating the spatial patterns of tumor-associated collagen signatures (TACS) which correlate with benign growth or invasive migration[43]. Models also aid in understanding the process of cancer cell metastasis as cells migrate through the ECM and extravasate into vasculature[44].

In summary, stochastic birth-death-migration models are commonly used to model tumor growth dynamics, often with a focus on deriving approximations that map local interaction dynamics to global mean-field approximations. Alterations in cell migration, proliferation, and death parameters may lead to spatial heterogeneity in cell density, reducing the accuracy of naive mean-field approximations. Thus, it's convenient for a cancer modeling framework to include 1) non-spatial or spatial, 2) deterministic or stochastic, and 3) single or multiple populations (cell types). Below, we illustrate how the Lenia mathematical framework integrates each of these components. Next, we illustrate how classical growth dynamics models (e.g. logistic growth) are a special case of Lenia. Then, we illustrate how multi-channel Lenia can be used to model cell-cell (tumor-immune) interactions. Finally, we show particle Lenia as an example of immune cell trafficking in cancer.

2   Results

2.1   Increased range of interaction increases tumor diffusivity and speeds growth

First, we implement a single population (one cell type) model of tumor growth dynamics in figure 2. Growth dynamics are described by logistic growth with an Allee threshold (Methods, eqn. 4), such that tumors seeded above the Allee threshold have positive growth. The solution to this ordinary differential equation is shown in blue in figure 2A. Comparing deterministic Lenia (figure 2A; solid lines) illustrates that systematically reducing the effective range of the interaction kernel reduces the rate of growth, and alters the temporal dynamics. Smaller interaction kernels (e.g. black lines) are characterized by slow growth due to the presence of contact inhibition in small interaction neighborhoods.

Reduction in kernel size (different kernel sizes used in figure 2B are shown in figure 2D) also alters the spatial variegation of tumor density. For example, short-range kernels (figure 2B, left) are characterized by sharp, well-defined boundary drive growth while long-range kernels (figure 2B, right) are associated with diffuse patterns.
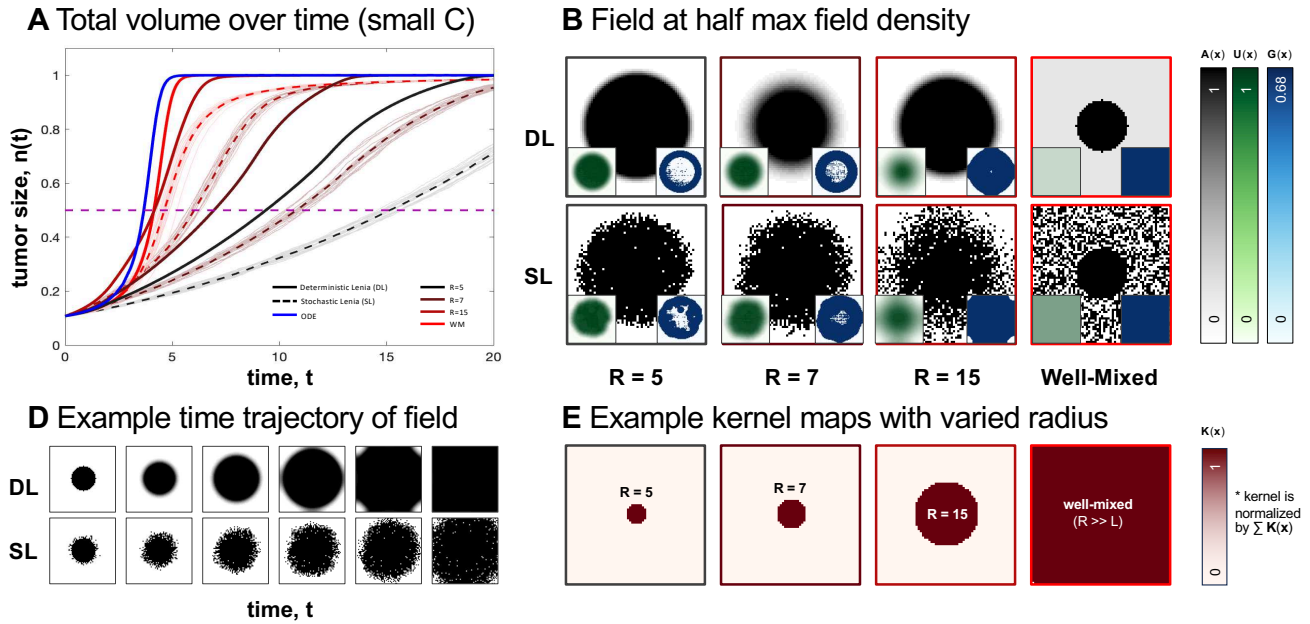
Figure 2. Cancer growth dynamics in Lenia (A) Average cell density over time for varying kernel sizes, for deterministic and stochastic Lenia. Averages over stochastic runs are shown in dotted lines and individual trajectories are shown in translucent lines. ODE solution (shown in blue) matches simulation with a well-mixed kernel. (B) State of field at half maximal capacity for different kernel sizes for Stochastic Lenia (SL) or Deterministic Lenia (DL). Density potential and Growth distribution shown in inset. (C) State of field at progressive time points for kernel size 4 for deterministic and stochastic Lenia. (D) Kernels used in models in figures (B).

This pattern holds when considering either a deterministic (figure 2B; Deterministic Lenia, DL) or a stochastic (figure 2B; Stochastic Lenia, SL) update rule (see Supplemental section S6.2). The average of many stochastic realizations is shown in dashed lines (figure 2A), which tend to underestimate the deterministic simulation with the corresponding kernel size. This is due in part to the fact that the cell density map $\mathbf{A}(\mathbf{x})$ in stochastic Lenia is restricted to integer values only, which is common practice in standard agent-based models (compare figure 2B, where only values of 0 or 1 are allowable). These results illustrate the utility of Lenia to interpolate between two standard modeling approaches: 1) ordinary differential equations and 2) stochastic, local agent-based methods. Lenia extends standard methods to allow investigation of arbitrary interaction kernels.
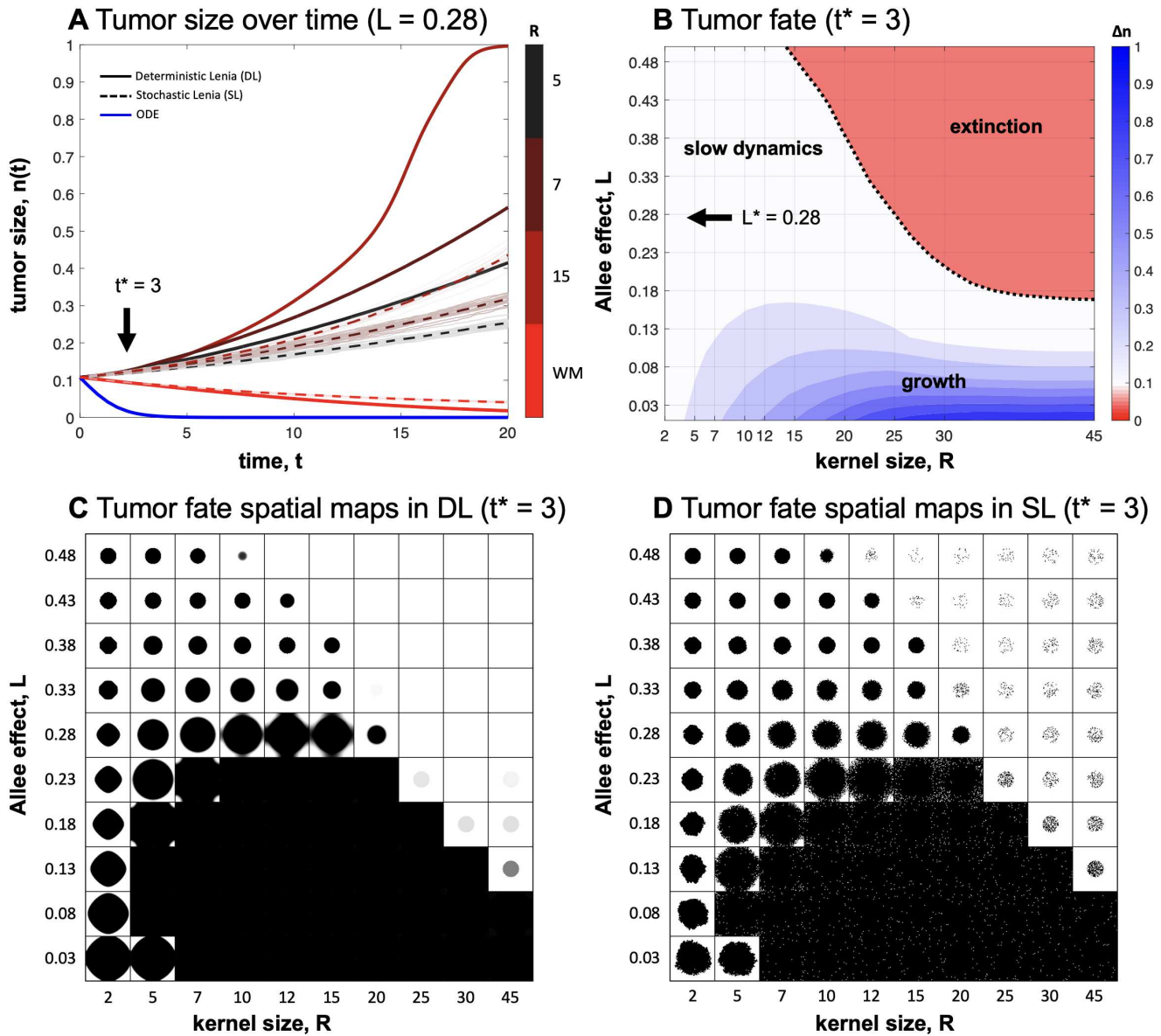
2.2 Short-range interaction kernels are more robust to Allee effects

Next, we investigate the interplay between the Allee threshold and the interaction kernel. Logistic growth with an Allee threshold has an unstable equilibrium which drives the population to extinction when tumor density is below the threshold. As shown in figure 3A, simulating logistic growth with Allee in an ODE (blue line) or a well-mixed (red line; WM) both result in eventual extinction. Interestingly, reducing the interaction kernel distance, R, results in positive tumor growth (e.g. black line). This effect occurs for a range of Allee threshold values and kernel sizes, shown in figure 3B. This clearly illustrates an expanded region of positive growth when kernel size is low, across a wide range of threshold values. Smaller neighborhoods increase the likelihood that a single cell's neighborhood will maintain a sufficient density above the Allee threshold, and thus maintain positive growth.

While stochastic Lenia is typically associated with slower temporal scales (figure 3A, dashed lines), the

long-term tumor fate (extinction or growth) are analogous in both models and spatial variegation patterns are also similar (figure 3C,D). These results suggest that well-mixed model formulation may overestimate the role of an Allee effect (thus overestimating the likelihood tumor extinction). In the next section, we investigate the effect of interaction kernel size on immune predation of tumors.

Figure 3. Short-range interaction kernels are more robust to Allee effects (A) Average cell density over time for varying kernel sizes, for deterministic and stochastic Lenia. Averages over stochastic runs are shown in dotted lines and individual trajectories are shown in translucent lines. ODE solution shown in blue. (B) Long-term tumor fate for deterministic Lenia where trajectories that eventually result in extinction are shown in red, or growth shown in blue (colorbar indicates change in tumor size at $t^* = 3$. (C, D) Spatial maps shown for deterministic Lenia (C) and stochastic Lenia (D) at time $t^* = 3$. See corresponding Supplementary Video S2.
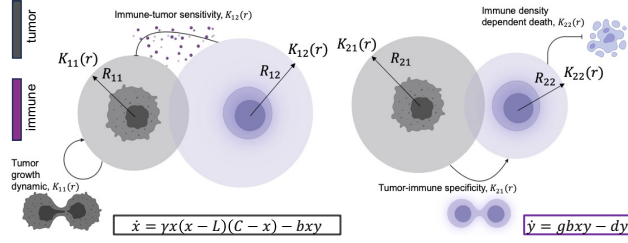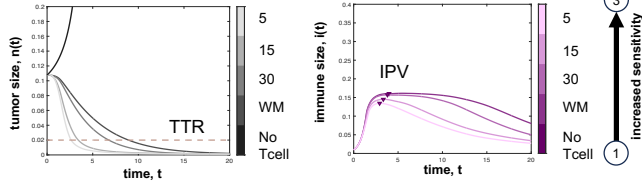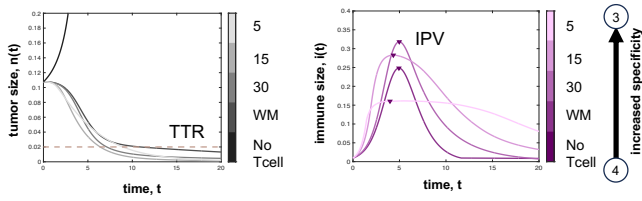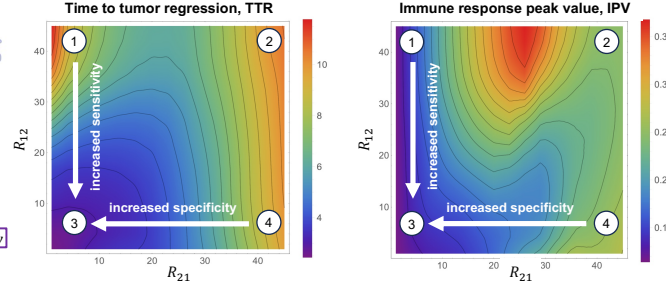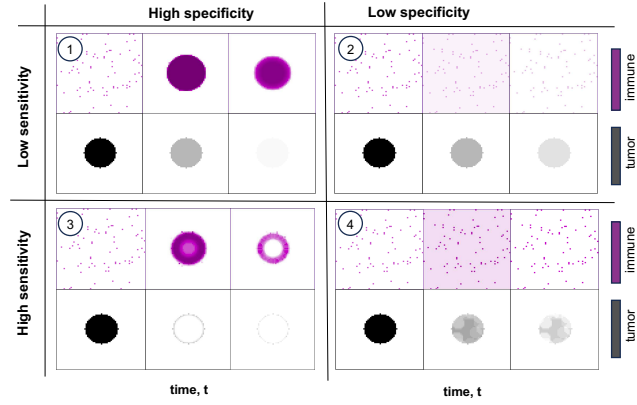
Figure 4. Competition dynamics in Lenia (A) Schematic representation of the tumor-immune predator-prey model, illustrating various kernel sizes for tumor growth (K_{11}), predation distance (K_{12}), immune recruitment (K_{21}), and density-dependent death distance in the immune system (K_{22}). (B, C) Impact of different predation distances (K_{12}) and immune recruitment (K_{21}) on the integration results of the tumor-immune predator-prey model, with other kernels held well-mixed. (D) Effect of varying predation and recruitment (K_{12} and K_{21}) on the time to tumor regression (considered when there are 2% tumor cells in the area) and the peak value in the immune response. (E) Spatial outcomes of the tumor and immune response in the model, showcasing the influence of different kernel sizes. See corresponding Supplementary Video S3. Unless otherwise noted, parameters used are $\gamma = 5, b = 12, g = 1.5, d = 1, L = 0.08$ (see eqns. 6-7).

2.3 High immune specificity and sensitivity maximize tumor regression

In order to investigate the effect of short-range and long-range interactions between tumor and immune cells, we employ the multi-channel Lenia model to simulate the dynamics of in a tumor-immune (figure 4). Tumor-immune dynamics are described by the predator-prey model in eqns. 6 and 7. Similar to the previous figure, this model contains an Allee threshold whereby tumor cells are driven to extinction below this threshold even in the absence of immune cells[37].

We consider four interaction kernels: tumor-tumor, tumor-immune, immune-tumor, and immune-immune (figure 4A). We define the tumor-immune kernel (K_{12}) as the **immune sensitivity**, whereby a short-range K_{12} is characterized by an increase in immune kill rate and decreasing the time to tumor regression (TTR) as seen in figure 4B. To gain intuition, one can consider the tumor-immune kernel as representing the average distance traveled by an immune cell per unit of tumor kill. For example, a large tumor-immune kernel may be represent a tumor with high PD-L1 expression, requiring immune cells to travel a further distance before effective immune activity.

Next, we define the immune-tumor kernel as the **immune specificity**, whereby a short-range K_{21} leads to more localized recruitment of immune cells in close proximity to tumor cells. A reduction in the recruitment distance (small K_{21}) leads to the production of an immune response in closer proximity to tumor cells (refer to figure 4E). To gain intuition about the immune-tumor kernel, one can consider this

A Image analysis to computational model pipeline
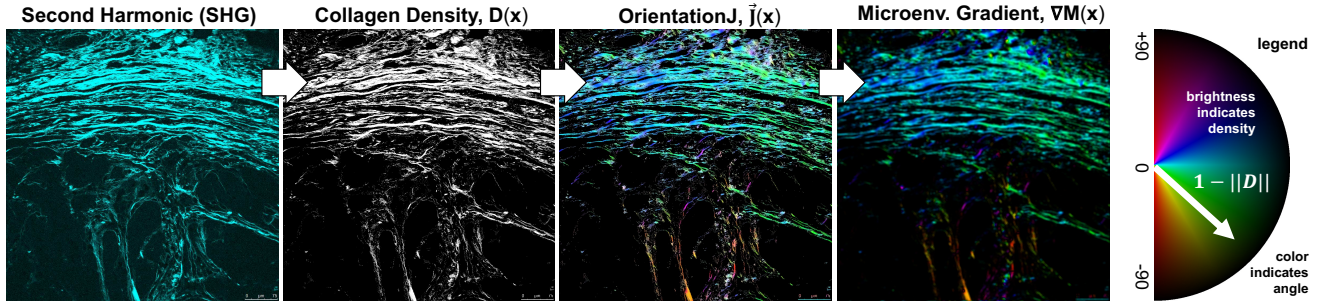
B Quantification of collagen alignment in HNSCC by disease stage
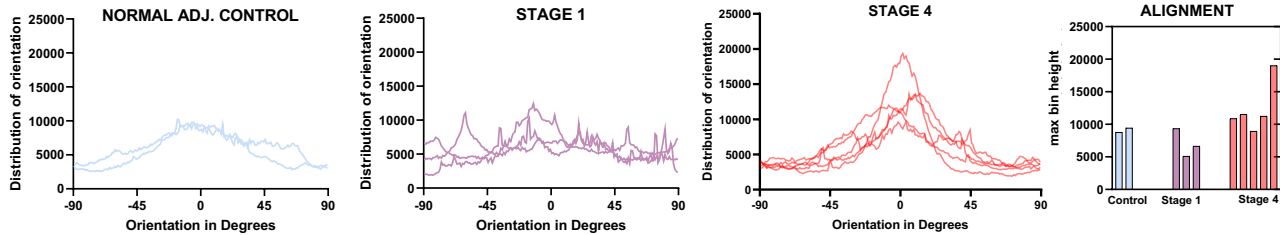
Figure 5. Collagen alignment in HNSCC (A) Pipeline of image analysis to computational model using second harmonic generation to determine collagen density and subsequently the alignment and microenvironmental gradient. (B) Alignment collagen fibers is determined using OrientationJ ImageJ plugin[45]; alignment tends to increase by disease stage.

kernel as representing the average distance an immune cell is recruited by a tumor. An immunologically quiet tumor is represented by a large kernel with diffuse, undirected recruitment, while increased tumor antigenicity is represented by a small kernel with strong, localized recruitment. The resulting immune peak value, IPV (figures 4B, C) depends on both **immune sensitivity** and **immune specificity**.

As seen in figure 4D, both immune specificity and immune sensitivity are required to maximize tumor regression (case 3). This effect is illustrated by observing spatial maps over time in figure 4E. High specificity results in rapid recruitment concentrated within the tumor, but these immune cells are most effective at removing tumor when sensitivity is high (case 3). In contrast, low specificity results in a diffuse spatial pattern of immune recruitment through the domain, where most immune cells are not co-localized with tumor cells, effectively wasting a majority of immune response (cases 2 and 4). Consequently, immune cells that do infiltrate tumor are rare but strongly effective, leading to a heterogeneous tumor kill (case 4). The effect of asymmetric interaction kernels leading to differences in spatial variegation and patterning in tumor and immune cells is shown for a range of sensitivity and specificity values in supplemental figure S1.

2.4 Stage-dependent collagen alignment predicts poor immune infiltration

Finally, we illustrate an example of a cell migration model using an extension of Particle Lenia[8]. In figure 5A, we introduce an image analysis to computational model pipeline. Second harmonic generation (SHG) is performed on a cohort of squamous cell carcinomas to quantify collagen density, $\mathbf{D}(\mathbf{x})$. Each patient has a selected region of interest (ROI) to perform SHG that are subsequently analyzed using OrientationJ ImageJ plugin to determine alignment, $\vec{\mathbf{J}}(\mathbf{x})$[45]. Each pixel is color-coded according to the directionality of collagen fibers, such that fibers aligned in a single direction are colored with the same hue on the red-blue-green-yellow spectrum (figure 5A, semi-circle legend color-bar). The microenvironment gradient field, $\nabla\mathbf{M}(\mathbf{x})$ at each grid location $\mathbf{x}$ is determined by the convolution of interaction kernel and the OrientationJ vector field, weighted by collagen density (see Methods). Thus, immune cells move in the same direction

as collagen fiber alignment. Similar to previous sections, immune cell movement direction is determined by the average collagen fiber alignment within the immune cell's interaction kernel radius, R.

Quantification of collagen alignment by disease stage

Late-stage head and neck squamous cell carcinomas (HNSCC) are associated with increased deposition and alignment of fibrillar collagens[46]. We hypothesize that poor outcomes are partially due to poor immune cell infiltration caused by deposition of a dense collagen barrier. Imaging data are quantified by stage in figure 5B, which illustrates the correlation of disease stage with collagen density and alignment. Normal adjacent control tissue and early stage HNSCC's are associated with sparse and heterogeneous collagen alignment, while late-stage HNSCC tends to contain highly aligned collagen fiber patches. We hypothesized that late-stage disease is associated with collagen structures which lead to poor immune infiltration. Thus, we next employed Lenia to test two plausible cell migration models describing the movement of immune cells in response to collagen: parallel or perpendicular movement.

Simulated effect of collagen alignment on immune surveillance

Within the immune cell trafficking model each simulated immune cell moves along a microenvironment gradient field determined by collagen fiber alignment (Methods; eqn. 8). Direct observation of immune cell trafficking patterns is unlikely in clinical tumors, but computational simulations based on clinical data can provide insight to test hypotheses. For example, we consider two hypothesized models of the influence of collagen fiber alignment on immune cell trafficking: perpendicular or parallel to collagen fibers (figure 6A). Immune cells are initially evenly distributed on the edge of the domain, and we quantify the area of surveillance covered (simplified example shown for six immune cells per side in figure 6B). The total simulated time is chosen such that immune cells in an empty domain would migrate in a linear, unaltered fashion and provide 100% coverage of the domain.

Results indicate an overall higher level of immune coverage in the perpendicular model than in parallel (figure 6C and D, respectively). Interestingly, the parallel model shows a stronger anti-correlation between immune coverage and disease stage. All stage 4 patients rank lower in immune coverage compared to patients with stage 1 tumors (figure 6D). Of note, it's difficult to interpret immune coverage for control tissues as the absence of immune infiltrates may result from lower collagen density typical of normal tissue and that is not well-aligned, or it could simply be due to absence of diseased tissue (i.e., tumor) and thus the absence of signaling cues required to induce immune cell trafficking. Late-stage HNSCC tumors are associated with a more hypoxia-related signature characterized by a low ratio of CD8+ T cells to FOXP3+ regulatory T cells,[47]. Thus, as the parallel model consistently predicts lower immune coverage for late-stage tumors, this model may be more biologically relevant. This also supports previous experimental findings that suggest immune cells move parallel to collagen structures[48]. Studies have shown that collagen fibers are often perpendicular to the outer boundary of tumors[49,50], suggesting that a parallel model of immune migration would reduce immune infiltration into the tumor. This finding supports the notion of the parallel immune migration model as a method of immune escape. Note: we do not consider variable immune response here (which may vary with disease stage) as the total number of immune cells seeded is constant across all patient simulations.

Individual model simulations are shown for a model seeded with corresponding collagen ROI (figure 6E). Immune cells are seeded along each edge (left, right, top, bottom) of the domain ($N = 5$ cells per pixel; figure 6F). Typically, as disease stage increases (left to right), immune cell coverage decreases as seen in figure 6G. We define immune coverage as the percentage of the domain covered (100% corresponds to pixels which are covered by at least one immune cell trafficked from each of the four sides). Well-aligned
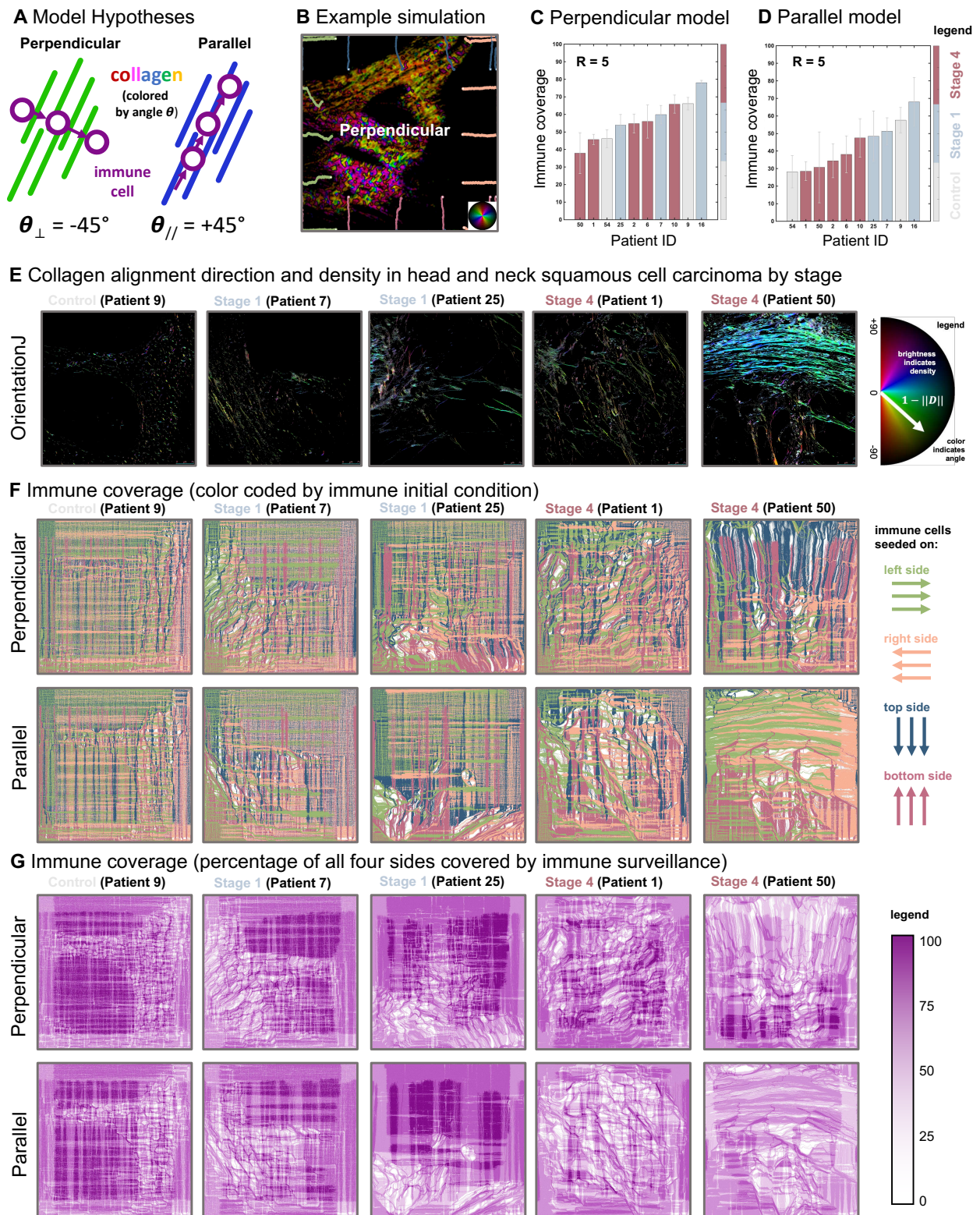
Figure 6. Immune cell trafficking model in Particle Lenia (A) Hypothesized models of the influence of collagen fiber alignment on immune cell trafficking. See corresponding Supplementary Video S4. (B) example simulation showing immune cell infiltration (circles) with track indicating path taken. Cells seed on all four sides, color-coded by initial side (see panel F). (C, D) Simulated immune coverage for perpendicular (C) or parallel (D) immune trafficking model, colored by stage. (E) Representative sample ROI alignment and density of collagen fibers (using OrientationJ ImageJ plugin[45]) ordered by disease stage. (F) Immune coverage, color coded by immune initial condition of which of the four sides: left, right, top, bottom (see legend). The color of each pixel is determined the most trafficked side. (G) Immune coverage as the percentage of all four sides covered by immune surveillance. For example, if no immune cells reached this pixel it is white, if all four sides reached this pixel, it is dark purple. See corresponding Supplementary Video S5.

collagen structures (e.g. stage 4) result in a strongly directed migration, deviating immune cells from providing a well-mixed coverage of the domain.

3   Discussion

Lenia demonstrates the capability to recapitulate important features required for modeling the evolution and ecology of cancer: growth dynamics (deterministic/stochastic), cell-cell interactions, and cell migration. While here we focus here on modeling tumor-immune spatial interactions, the role of spatial structure more broadly has important implications for optimizing cancer treatment[51,52], modulating evolutionary dynamics of tumor heterogeneity[17,19,53], and altering cell-cell competitive dynamics[54] even when using the same interaction rules[55,56]. Lenia is flexible enough to mimic non-spatial (well-mixed) ordinary differential equations (with sufficiently large kernel sizes) as well as small-scale spatial neighborhoods commonly used in agent-based methods (e.g. Moore or von Neumann neighborhoods). It is also straightforward to simulate deterministic dynamics and the corresponding stochastic dynamics. Additionally, Lenia can simulate ecological interactions between multiple cell types in heterogeneous tumors. We have shown the ability of Lenia to recapitulate common models of tumor-immune dynamics (logistic-Allee). Finally, we illustrate the ability of Particle Lenia to recapitulate cell migration and trafficking in an off-lattice, with an application in squamous cell carcinomas. However, Lenia provides several natural advantages over traditional birth-death-migration models. Kernel convolution can be performed using fast-Fourier transforms, drastically decreasing the computational cost of simulations. Additionally, convolution of extrinsic migration gradient can be pre-computed, increasing computational efficiency.

In addition to flexible methodology, Lenia has shown promise in understanding the mechanics of tumor-immune interactions. We have illustrated that short-range interaction kernels provide a mechanism for tumor cell survival under conditions for strong Allee effects (figure 3). We have also shown the importance of both immune sensitivity and specificity in immune response (figure 4). In the absence of either, poor immune response leads to prolonged tumor growth and in some cases, immune escape. Differential interaction kernels alter the spatial patterns of tumor-immune cells (figure S1), leading us to hypothesize the possibility of making inferences of kernel sizes based on spatial co-localization of cells in future works. Here, we may draw inspiration from literature in ecology where kernel inferences are drawn from plant seed dispersal patterns[57]. Finally, we have shown the ability of Lenia to reproduce immune-ECM interactions where patterns of collagen formation evolve as a mechanism of immune escape (figure 5). Previously, aligned collagen fibers have been observed perpendicular to the tumor periphery[49,50], lending supporting evidence to a parallel model of immune migration that reduces immune infiltration. Despite neglecting alternative mechanisms of immune escape (e.g. acid-inactivation, immune checkpoint expression, or immune exhaustion), the immune infiltration model shows an inverse relationship between disease stage and immune coverage as an emergent phenomenon (figure 6).

4 Methods

4.1 Lenia Cellular Automata

The notation here follows ref. 1, which we re-state here for clarity. Lenia is a cellular automata defined by five components: 1) a discrete grid of points, $\mathscr{L}$, (herein we consider two-dimensional lattice grid $\mathscr{L} \in \mathbb{R}^2$), 2) the range of allowable states $\mathscr{S} = [A_{\min}, A_{\max}]$, 3) the local update rule $\phi : \mathscr{S}^{\mathcal{N}} \to \mathscr{S}$ is the local update rule, 4) the neighborhood around each focal cell at location $\mathbf{x}$, given by $\mathcal{N}_{\mathbf{x}} = \{\mathbf{x} + \mathbf{n} : \mathbf{n} \in \mathcal{N}\}$, and 5) time steps $t \in \mathcal{T}$. The spatial *cell density* map configuration is defined by $\mathbf{A}^t : \mathscr{L} \to \mathscr{S}$: the collection of states over the whole grid, at time $t \in \mathcal{T}$, the timeline. Herein, we let $\mathbf{A}$ be a two-dimensional matrix where $\mathbf{A}(\mathbf{x})$ represents the cell density at grid location $\mathbf{x}$ which is updated via the following equation:

$$\mathbf{A}^{t+\Delta t}(\mathbf{x}) = \left[\mathbf{A}^t(\mathbf{x}) + G(\mathbf{U}^t(\mathbf{x}))\Delta t\right]_{A_{\min}}^{A_{\max}} \tag{1}$$

where $G(u)$ is the density-dependent growth function defined on the interval $u \in [A_{\min}, A_{\max}]$. For each point $\mathbf{x}$, the convolution of a kernel $\mathbf{K}$ with $\mathbf{A}^t(\mathcal{N}_{\mathbf{x}})$ is calculated to compute the potential distribution $\mathbf{U}^t$:

$$\mathbf{U}^t(\mathbf{x}) = \mathbf{K} * \mathbf{A}^t(\mathbf{x}) = \sum_{\mathbf{n} \in \mathcal{N}} \mathbf{K}(\mathbf{n}) \cdot \mathbf{A}^t(\mathbf{x} + \mathbf{n}) \tag{2}$$

Thus, the growth is defined at every lattice location: $\mathbf{G}^t(\mathbf{x}) := G(\mathbf{U}^t(\mathbf{x}))$. A fraction of the growth distribution is added to each site at each time step (Euler approximation update rule) and the value at the site is clipped to $[A_{\min}, A_{\max}]$. We implement the computational model in the Hybrid Automata Library framework (Java)[58].

4.2 Interpretation of Lenia as a cancer model

Next, we make explicit the connection to cancer modeling. Lenia provides a natural framework for constructing mathematical models of cancer cell growth, competition, and migration, where each lattice location $\mathbf{x}$ contains a density of tumor cells, $\mathbf{A}^t(\mathbf{x})$. When modeling tumor dynamics, set $A_{\min} = 0$ and $A_{\max} = C$ where C represents the maximum resource- or space-limited carrying capacity of cells within each single lattice location. Classic cell interaction neighborhoods such as von Neumann (the four nearest neighbors; $R = 1$) or Moore (eight nearest neighbors; $R = 1.8$) can be written as an interaction kernel function, defined as a circle of radius R:

$$K(r) = \varepsilon \cdot (1 - H(R - r)) \tag{3}$$

where H is the Heaviside function, and ε is chosen to normalize the elements of the kernel to sum to one. Thus, $\mathbf{U}(\mathbf{x})$ represents a potential density that is perceived by the focal location, determining the location-specific growth rate of cells, $G(\mathbf{U}(\mathbf{x}))$. The density potential is the convolution of cell density within the neighborhood, $\mathbf{A}(\mathcal{N}_x)$, weighted (convolved) by the values in the kernel function. Typical kernel functions in cancer modeling are likely to be non-increasing functions of the radial distance from the focal location. For notational convenience, define the mean density of the field as $\hat{n}(t) = \frac{1}{\|\mathscr{L}\|} \sum_{\mathbf{x} \in \mathscr{L}} \mathbf{A}^t(\mathbf{x})$, where $\|\mathscr{L}\|$ is the total number of lattice locations in domain $\mathscr{L}$.

Lenia can be extended to a stochastic setting by restricting only integer values on each lattice point ($\mathbf{A}(\mathbf{x}) \in [0, 1, 2, \ldots, A_{\max}]$) with stochastic updates (see Supplemental Section S6.2). We note that classic

agent-based methods often restrict each lattice location to contain at most a single cell ($A_{\max} = 1$) and make the implicit assumption that cells divide into surrounding empty locations with probability b. This is qualitatively similar to defining a Moore-like or von Neumann-like interaction kernel with $G(\mathbf{U}(\mathbf{x})) = b$.

4.2.1 Tumor growth dynamics model

We first model tumor growth as a local logistic growth dynamic, shown in figure 1E, and F given by:

$$G(u) = \gamma u (C - u)(u - L) \tag{4}$$

where γ is the intrinsic growth rate of tumor cells, C is the carrying capacity (maximum density) of each lattice location, L is the allee effect, and u is the density potential (eqn. 2).

4.2.2 Tumor-immune predator-prey model

Using multi-channel Lenia, we can extend the model to account for cell density of multiple cell types, $\mathbf{A}_i(\mathbf{x})$ where $i \in \{1, 2, \ldots, N\}$. For example, herein we consider competition between $N = 2$ cell types that each have a growth field which is a function of the density potential for both cell types: $\mathbf{G}_i^t(\mathbf{x}) := G_i(\mathbf{U}_1^t(\mathbf{x}), \mathbf{U}_2^t(\mathbf{x}))$. In this two-type case, the dynamics are given by:

$$\mathbf{A}_i^{t+\Delta t} = \left[\mathbf{A}_i^t + G_i \left(\mathbf{U}_{i1}^t(\mathbf{x}), \mathbf{U}_{i2}^t(\mathbf{x}) \right) \Delta t \right]_{A_{i,\min}}^{A_{i,\max}} \tag{5}$$

Thus, the tumor-immune model can be written as a system of two growth functions:

$$\underbrace{G_1(u_{11}, u_{12})}_{\text{tumor (prey)}} = \underbrace{\gamma u_{11}(u_{11} - L)(C - u_{11})}_{\text{logistic growth with Allee}} - \underbrace{bu_{11}u_{12}}_{\text{predation}} \tag{6}$$

$$\underbrace{G_2(u_{21}, u_{22})}_{\text{immune (predator)}} = \underbrace{g(bu_{21}u_{22})}_{\text{predator growth}} - \underbrace{du_{22}}_{\text{natural death}} \tag{7}$$

where u_{ij} represents the density of cell type j perceived by cell type i. The Allee threshold is given by L, carrying capacity of tumor cells is C, and predation rate is b. Immune cells and expand at rate g (weighted by immune predation response) and die at rate d.

Modeling cell migration using Particle Lenia

A recent extension referred to as Particle Lenia extends the mathematical framework to off-lattice. The location of each cell i is given by vector $\mathbf{p}_i := \{x, y\}$ corresponding to its location in two-dimensions. Movement of the particle is determined by the local gradients of the energy and chemotactic migration fields: $\mathbf{E}(\mathbf{p}_i)$ and $\mathbf{M}(\mathbf{p}_i)$, respectively.

$$\frac{d\mathbf{p}_i}{dt} = \underbrace{-\nabla \mathbf{E}(\mathbf{p}_i)}_{\text{cell adhesion-repulsion}} + \underbrace{\nabla \mathbf{M}(\mathbf{p}_i)}_{\text{microenvironment}} = -\frac{\partial \mathbf{E}(\mathbf{p}_i)}{\partial (\mathbf{p}_i)} + \frac{\partial \mathbf{M}(\mathbf{p}_i)}{\partial (\mathbf{p}_i)} \tag{8}$$

Particles (i.e. cells) in this model move against the local gradient of the energy field, representing particle interactions[a]. The cell-cell repulsion and adhesion fields are a function of the potential field, $\mathbf{E}^t(\mathbf{x}) = E(\mathbf{U}^t(\mathbf{x}))$ (see Supplemental info section S6.3). Similarly, an extrinsic microenvironmental field $\mathbf{M}(\mathbf{p}_i)$, defines the chemotactic direction of cells moving toward a nutrient-based or bio-mechanical gradient. The cell position update rule can be deterministic (following the highest point of gradient) or stochastic (weighted in the direction of gradient).

Modeling the effect of collagen on T-cell migration

In this manuscript, we assume negligible T-cell adhesive-repulsive interactions such that $E(\mathbf{U}^t(\mathbf{x})) = 0$. Instead, T-cells move in a directed fashion influenced by the surrounding extrinsic microenvironment according to the following equation:

$$\nabla \mathbf{M}(\mathbf{p}_i) \quad = \quad \mathbf{K} * \vec{\mathbf{C}}^t(\mathbf{x}) \tag{9}$$

where $\mathbf{K}$ is the cell-microenvironment interaction kernel (see eqn. 3), $\vec{\mathbf{C}} = \{||C||, \theta\}$ is a vector field determined by collagen fiber alignment. At each time point, noise is added to the collagen vector field's angle such that $\theta' = \theta + R(\sigma)$ where R is a uniform random variable on $[0, \sigma]$ radians.

In this way, we model the influence of collagen fibers to direct T-cell movement as a weighted vector summation of the collagen fiber alignment in the focal T-cell's local neighborhood. The collagen fiber alignment vector field is inversely proportional to the density of collagen (cells travel slowly in dense fibers). We consider two plausible models of the influence of collagen on T-cell migration: T-cells travel 1) in parallel to collagen fibers or 2) perpendicular to collagen fibers, denoted $\parallel$ and $\perp$, respectively.

$$\vec{\mathbf{C}}(\mathbf{x}) \quad = \quad (1 - \mathbf{D}(\mathbf{x}))\vec{\mathbf{J}}_\perp(\mathbf{x}) \tag{10}$$
$$\vec{\mathbf{C}}(\mathbf{x}) \quad = \quad (1 - \mathbf{D}(\mathbf{x}))\vec{\mathbf{J}}_\parallel(\mathbf{x}) \tag{11}$$

where $\vec{\mathbf{J}}(\mathbf{x})$ is collagen fiber alignment (a unit vector) derived from clinical imaging, detailed in the next section below, scaled by the inverse of the normalized density of collagen at each grid location, $\mathbf{D}(\mathbf{x}) \in [0, 1]$.

Immune cell migration field defined using OrientationJ

Tumor microarray (TMA) having FFPE tissue samples from HPV-negative HNSCC patient cohort from the H. Lee Moffitt Cancer Center and Research Institute (IRB: MCC#18754) was analyzed to determine collagen alignment in the tumor microenvironment. The TMA cores were imaged using a Leica SP5 AOBS multiphoton confocal microscope and a 25x, HC IR Apo, NA 0.95 water immersion objective. The excitation wavelength was tuned to 880 nm and emitted light was detected at 440 nm using bandpass filters for detecting the SHG signal of collagen. The SHG images were analyzed using the Orientation J plugin[45] in ImageJ software which provides both visual and quantitative data outputs for collagen fiber alignment[60].

---

[a]For example, one might define $\mathbf{E}$ as the Lennard-Jones potential function, which describes the balance of repulsive and attractive forces as a function of the distance between two interacting particles[59]

5 Acknowledgments

S6 Supplemental Information

S6.1 Spatial variegation of tumor-immune interactions

We assess the degree of spatial variegation and patterning in tumor and immune cells as a function of sensitivity and specificity in figure S1. Spatial maps are shown at time to tumor regression (TTR; see figure 4), and thus all tumors have identical total size in figure S1A. Differences in spatial patterns of tumor density are caused by differential immune recruitment (specificity) and strength of predation (sensitivity). As the immune specificity narrows (r_{21} reduces to smaller values), immune cell concentration strongly correlates with the tumor's location with a high degree of specificity (figure S1B, right-to-left). This specificity has only a marginal effect on tumors if the range of sensitivity is diffuse (large r_{12} values). As sensitivity narrows, immune predation is more highly targeted and effective, killing tumor cells, especially in the core (figure S1A, bottom-left). A ring-shaped tumor is left, due to proliferating cells on the rim.

A Tumor spatial dynamics at t = TTR   **B** Immune spatial dynamics at t = TTR
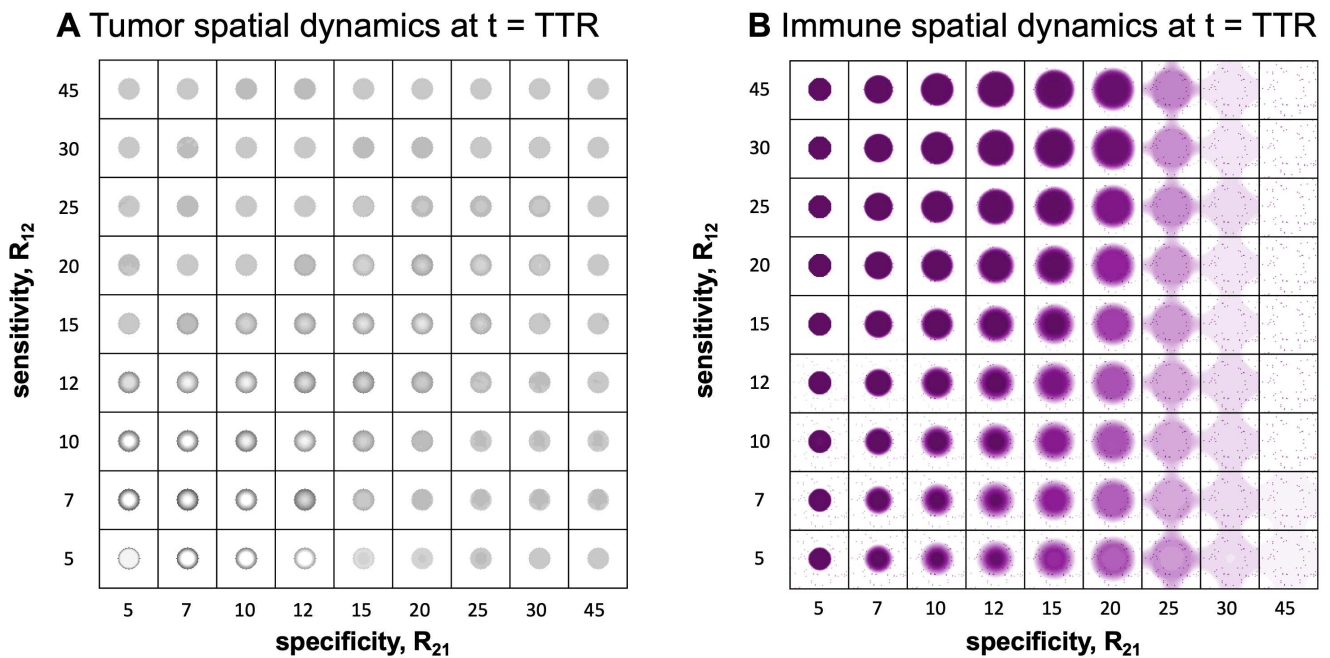
Figure S1. Tumor-immune spatial variegation patterns as a function of interaction kernels Spatial maps are shown at the time to tumor regression (TTR; see figure 4) for a range of tumor-immune sensitivity (r_{12}) and specificity (r_{21}) values. (A) Tumor spatial maps at TTR. (B) Immune spatial maps at TTR. Spatial variegation in tumor density increases as both specificity and sensitivity are increased. As immune specificity narrows (r_{21} is small), immune cell concentration strongly correlates with tumor's location with a high degree of specificity. Unless otherwise noted, parameters used are $\gamma = 5, b = 12, g = 1.5, d = 1, L = 0.08$ (see eqns. 6-7).

S6.2 Stochastic Lenia

The Lenia framework can be extended to a stochastic setting by considering the likelihood of a lattice location $\mathbf{x}$ containing a single cell. Let $\mathbf{A}(\mathbf{x}) \in [0,1]$ be a random variable, such that the probability, P, of a cell potentially being added to an existing lattice location $\mathbf{x}$ at the next time step $t + \Delta t$. This probability is determined by the Binomial distribution (if the lattice location is currently empty), at a rate of $G(\mathbf{U}(\mathbf{x}))\Delta t$.

S6.3 Particle Lenia

Particle Lenia is an extension of Lenia where movement of the particle is determined by the sum of two local gradients representing the energy field, $\mathbf{E}(\mathbf{p}_i)$, and migration field, $\mathbf{M}(\mathbf{p}_i)$. Particle i's location in two-dimensional space is given by $\mathbf{p}_i := \{x, y\}$ and updated according to the following equation:

$$\frac{d\mathbf{p}_i}{dt} = \underbrace{-\nabla\mathbf{E}(\mathbf{p}_i)}_{\texttt{cell adhesion-repulsion}} + \underbrace{\nabla\mathbf{M}(\mathbf{p}_i)}_{\texttt{microenvironment}} = -\frac{\partial\mathbf{E}(\mathbf{p}_i)}{\partial(\mathbf{p}_i)} + \frac{\partial\mathbf{M}(\mathbf{p}_i)}{\partial(\mathbf{p}_i)} \tag{12}$$

Particles (or cells) move against the local gradient of $\mathbf{E}(\mathbf{x})$, the energy field. The cell-cell repulsion and adhesion fields are a function of the potential field, $\mathbf{U}$, such that:

$$\mathbf{E}^t(\mathbf{x}) = E\left(\mathbf{U}^t(\mathbf{x})\right) \tag{13}$$

$$= E\left(\sum_i \mathbf{K}\left(\mathbf{x} - \mathbf{p}_i^t\right)\right) \tag{14}$$

$$= E\left(\sum_i K\left(\|\mathbf{x} - \mathbf{p}_i^t\|\right)\right) \tag{15}$$

where $\mathbf{E}^t(\mathbf{x})$ is interpreted as the energy field as a function of the distance from the focal particle. Interacting cells move along the gradient of the energy field, weighted by the interaction kernel as a function of particle-particle distance, and summed over all particles.

S7 Supplemental Video Captions

Figure S2. Supplemental Video S1: Short-range interaction kernels are more robust to Allee effects Spatial maps shown for deterministic Lenia (left) and stochastic Lenia (right) over time.

Figure S3. Supplemental Video S2: tumor-immune spatial variegation patterns as a function of interaction kernels Video of simulations, corresponding to figure S1. Left: Spatial maps shown over time for a range of tumor-immune sensitivity (r_{12}) and specificity (r_{21}) values. Right: Immune spatial maps over time. Spatial variegation in tumor density increases as both specificity and sensitivity are increased. As immune specificity narrows (R_{21} is small), immune cell concentration strongly correlates with tumor's location with a high degree of specificity. Parameters used are $\gamma = 5, b = 12, g = 1.5, d = 1, L = 0.08$ (see eqns. 6-7).

Figure S4. Supplemental Video S3: example immune infiltration simulation for perpendicular and parallel model Video of simulations, corresponding to figure 6. Left: perpendicular model. Right: parallel model.

Figure S5. Supplemental Video S4: example immune infiltration simulation for perpendicular and parallel model Video of simulations, corresponding to figure 6E. Simulations ordered by disease stage from left to right.

References

1. Chan, B. W.-C. Lenia-biology of artificial life. *arXiv preprint arXiv:1812.05433* (2018).

2. Chan, B. W.-C. Lenia and expanded universe. In *Artificial Life Conference Proceedings 32*, 221–229 (MIT Press One Rogers Street, Cambridge, MA 02142-1209, USA journals-info . . . , 2020).

3. Jain, S. & Shrestha, A. Capturing emerging complexity in lenia. *arXiv preprint arXiv:2305.09378* (2023).

4. Gardner, M. Mathematical games-the fantastic combinations of john conway's new solitaire game, life, 1970. *Scientific American, October* 120–123.

5. Davis, Q. T. & Bongard, J. Glaberish: generalizing the continuously-valued lenia framework to arbitrary life-like cellular automata. In *Artificial Life Conference Proceedings 34*, vol. 2022, 47 (MIT Press One Rogers Street, Cambridge, MA 02142-1209, USA journals-info . . . , 2022).

6. Plantec, E. *et al.* Flow lenia: Mass conservation for the study of virtual creatures in continuous cellular automata. *arXiv preprint arXiv:2212.07906* (2022).

7. Kawaguchi, T., Suzuki, R., Arita, T. & Chan, B. Introducing asymptotics to the state-updating rule in lenia. In *ALIFE 2022: The 2022 Conference on Artificial Life* (MIT Press, 2021).

8. Horibe, K., Suzuki, K., Horii, T. & Ishiguro, H. Exploring the adaptive behaviors of particle lenia: A perturbation-response analysis for computational agency. *arXiv preprint arXiv:2305.16706* (2023).

9. Kojima, H. & Ikegami, T. Implementation of lenia as a reaction-diffusion system. *arXiv preprint arXiv:2305.13784* (2023).

10. Gerlee, P. The model muddle: in search of tumor growth laws. *Cancer research* **73**, 2407–2411 (2013).

11. Benzekry, S. *et al.* Classical mathematical models for description and prediction of experimental tumor growth. *PLoS computational biology* **10**, e1003800 (2014).

12. Ghaffari Laleh, N. *et al.* Classical mathematical models for prediction of response to chemotherapy and immunotherapy. *PLoS computational biology* **18**, e1009822 (2022).

13. Baker, R. E. & Simpson, M. J. Correcting mean-field approximations for birth-death-movement processes. *Physical Review E* **82**, 041905 (2010).

14. West, J. & Newton, P. K. Cellular interactions constrain tumor growth. *Proceedings National Academy Sciences* **116**, 1918–1923 (2019).

15. Kimmel, G. J., West, J., Damaghi, M., Anderson, A. R. & Altrock, P. M. Local contact inhibition leads to universal principles of cell population growth. *arXiv preprint arXiv:2108.10000* (2021).

16. Lewinsohn, M. A., Bedford, T., Müller, N. F. & Feder, A. F. State-dependent evolutionary models reveal modes of solid tumour growth. *Nature Ecology & Evolution* **7**, 581–596 (2023).

17. Noble, R. *et al.* Spatial structure governs the mode of tumour evolution. *Nature Ecology & Evolution* **6**, 207–217 (2022).

18. Streck, A., Kaufmann, T. L. & Schwarz, R. F. Smith: spatially constrained stochastic model for simulation of intra-tumour heterogeneity. *Bioinformatics* **39**, btad102 (2023).

19. West, J., Schenck, R. O., Gatenbee, C., Robertson-Tessi, M. & Anderson, A. R. Normal tissue architecture determines the evolutionary course of cancer. *Nature Communications* **12**, 2060 (2021).

20. Pérez-García, V. M. *et al.* Universal scaling laws rule explosive growth in human cancers. *Nature Physics* **16**, 1232–1237 (2020).

21. Jiménez-Sánchez, J. *et al.* Evolutionary dynamics at the tumor edge reveal metabolic imaging biomarkers. *Proceedings National Academy Sciences* **118**, e2018110118 (2021).

22. Deutsch, A. & Dormann, S. *Mathematical modeling of biological pattern formation* (Springer, 2005).

23. Ryser, M. D., Min, B.-H., Siegmund, K. D. & Shibata, D. Spatial mutation patterns as markers of early colorectal tumor cell mobility. *Proceedings National Academy Sciences* **115**, 5774–5779 (2018).

24. Hoshino, T. *et al.* Pattern formation of skin cancers: Effects of cancer proliferation and hydrodynamic interactions. *Physical Review E* **99**, 032416 (2019).

25. Calcaterra, C. & Boldt, A. Existence of life in lenia. *arXiv preprint arXiv:2203.14390* (2022).

26. Maddalena, L. Analysis of an integro-differential system modeling tumor growth. *Applied Mathematics Computation* **245**, 152–157 (2014).

27. Jain, H. V. & Byrne, H. M. Qualitative analysis of an integro-differential equation model of periodic chemotherapy. *Applied Mathematics Letters* **25**, 2132–2136 (2012).

28. Greene, J. M. *et al.* Modeling intrinsic heterogeneity and growth of cancer cells. *Journal theoretical biology* **367**, 262–277 (2015).

29. Bekker, R. A. *et al.* Rethinking the immunotherapy numbers game. *Journal for immunotherapy cancer* **10** (2022).

30. Hamilton, P. T., Anholt, B. R. & Nelson, B. H. Tumour immunotherapy: lessons from predator–prey theory. *Nature Reviews Immunology* **22**, 765–775 (2022).

31. Schiavo, M. L. Discrete kinetic cellular models of tumors immune system interactions. *Mathematical Models Methods Applied Sciences* **6**, 1187–1209 (1996).

32. Arlotti, L. & Lachowicz, M. Qualitative analysis of a nonlinear integrodifferential equation modeling tumor-host dynamics. *Mathematical computer modelling* **23**, 11–29 (1996).

33. Aylaj, B. Qualitative analysis and simulation of a nonlinear integro-differential system modeling tumor-immune cells competition. *International Journal Biomathematics* **11**, 1850104 (2018).

34. Kolev, M. Mathematical modelling of the competition between tumors and immune system considering the role of the antibodies. *Mathematical Computer Modelling* **37**, 1143–1152 (2003).

35. Lachowicz, M. & Quartarone, A. A general framework for modeling tumor-immune system competition at the mesoscopic level. *Applied Mathematics Letters* **25**, 2118–2122 (2012).

36. Alfonso, J. C. *et al.* Tumor-immune ecosystem dynamics define an individual radiation immune score to predict pan-cancer radiocurability. *Neoplasia* **23**, 1110–1122 (2021).

37. Kareva, I., Luddy, K. A., O'Farrelly, C., Gatenby, R. A. & Brown, J. S. Predator-prey in tumor-immune interactions: A wrong model or just an incomplete one? *Frontiers Immunology* **12**, 668221 (2021).

38. Brown, J. S., Cunningham, J. J. & Gatenby, R. A. Aggregation effects and population-based dynamics as a source of therapy resistance in cancer. *IEEE Transactions on Biomedical Engineering* **64**, 512–518 (2016).

39. Johnson, K. E. *et al.* Cancer cell population growth kinetics at low densities deviate from the exponential growth model and suggest an allee effect. *PLoS biology* **17**, e3000399 (2019).

40. Abhilash, A., Baker, B., Trappmann, B., Chen, C. & Shenoy, V. Remodeling of fibrous extracellular matrices by contractile cells: predictions from discrete fiber network simulations. *Biophys* **107**, 1829–1840 (2014).

41. Pruitt, H. C. *et al.* Collagen fiber structure guides 3d motility of cytotoxic t lymphocytes. *Matrix Biology* **85**, 147–159 (2020).

42. Suveges, S., Chamseddine, I., Rejniak, K. A., Eftimie, R. & Trucu, D. Collective cell migration in a fibrous environment: A hybrid multiscale modelling approach. *Frontiers Applied Mathematics Statistics* **7**, DOI: 10.3389/fams.2021.680029 (2021).

43. Poonja, S., Forero Pinto, A., Lloyd, M. C., Damaghi, M. & Rejniak, K. A. Dynamics of fibril collagen remodeling by tumor cells: A model of tumor-associated collagen signatures. *Cells* **12**, 2688 (2023).

44. Sabeh, F., Shimizu-Hirota, R. & Weiss, S. J. Protease-dependent versus-independent cancer cell invasion programs: three-dimensional amoeboid movement revisited. *Journal Cell Biology* **185**, 11–19 (2009).

45. Sage, D. Orientationj: A series of imagej plugins for directional image analysis. *Biomedical Image Group at EPFL, Switzerland* (2020).

46. Saito, T. *et al.* Aberrant collagen cross-linking in human oral squamous cell carcinoma. *Journal dental research* **98**, 517–525 (2019).

47. Chaudhary, R. *et al.* Egfr inhibition by cetuximab modulates hypoxia and ifn response genes in head and neck squamous cell carcinoma. *Cancer Research Communications* **3**, 896–907 (2023).

48. Sadjadi, Z., Zhao, R., Hoth, M., Qu, B. & Rieger, H. Migration of cytotoxic t lymphocytes in 3d collagen matrices. *Biophysical Journal* **119**, 2141–2152 (2020).

49. Conklin, M. W. *et al.* Aligned collagen is a prognostic signature for survival in human breast carcinoma. *Am J Pathol* **178**, 1221–32, DOI: 10.1016/j.ajpath.2010.11.076 (2011).

50. Rømer, A. M. A., Thorseth, M.-L. & Madsen, D. H. Immune modulatory properties of collagen in cancer. *Frontiers Immunology* **12**, DOI: 10.3389/fimmu.2021.791453 (2021).

51. Gallaher, J. A., Enriquez-Navas, P. M., Luddy, K. A., Gatenby, R. A. & Anderson, A. R. Spatial heterogeneity and evolutionary dynamics modulate time to recurrence in continuous and adaptive cancer therapies. *Cancer Research* **78**, 2127–2139 (2018).

52. Strobl, M. A. R. *et al.* Turnover modulates the need for a cost of resistance in adaptive therapy. *BioRxiv* (2020).

53. Dénes, A., Marzban, S. & Röst, G. Global analysis of a cancer model with drug resistance due to lamarckian induction and microvesicle transfer. *Journal Theoretical Biology* **527**, 110812, DOI: https://doi.org/10.1016/j.jtbi.2021.110812 (2021).

54. Hamis, S. *et al.* Spatial cumulant models enable spatially informed treatment strategies and analysis of local interactions in cancer systems. *Journal Mathematical Biology* **86**, 68 (2023).

55. Nowak, M. A. *Evolutionary Dynamics* (Harvard University Press, 2006).

56. You, L. *et al.* Spatial vs. non-spatial eco-evolutionary dynamics in a tumor growth model. *Journal Theoretical Biology* **435**, 78–97 (2017).

57. Bullock, J. M. *et al.* A synthesis of empirical plant dispersal kernels. *Journal Ecology* **105**, 6–19 (2017).

58. Bravo, R. R. *et al.* Hybrid automata library: A flexible platform for hybrid modeling with real-time visualization. *PLoS Computational Biology* **16**, e1007635 (2020).

59. Lennard-Jones, J. E. Cohesion. *Proceedings Physical Society* **43**, 461 (1931).

60. Franco-Barraza, J., Beacham, D. A., Amatangelo, M. D. & Cukierman, E. Preparation of extracellular matrices produced by cultured and primary fibroblasts. *Current protocols cell biology* **71**, 10–9 (2016).

Supplementary Files

This is a list of supplementary files associated with this preprint. Click to download.

- SuppVideo1.mp4
- SuppVideo2.mp4
- SuppVideo3.mp4
- SuppVideo4.mp4